MULTI-YEAR EFFECTS OF GLOBAL DUST STORMS ON THE POLAR HEAT BUDGET AND CO_2 SNOWFALL ON MARS.

P. O. Hayne, N. Alsaeed, V. Concepcion, *Laboratory for Atmospheric and Space Physics, University of Colorado Boulder (paul.hayne@colorado.edu)*, **D. M. Kass, S. Piqueux, J. Bapst, A. Kleinboehl,** *NASA - Jet Propulsion Laboratory, California Institute of Technology*.

Introduction

Planetary scale dust storms are known to have measurable, though typically short-lived effects on the climate and atmospheric circulation of Mars. Occurring on roughly decadal timescales, these global events increase planetary albedo, warm the surface at night, and transport water to high altitudes, contributing to its loss from the upper atmosphere [1, 2].

Here, we report multi-year impacts of dust storms on polar temperatures, CO_2 snowfall, and the extent and retreat of the seasonal polar caps. We focus primarily on the 2007 (Mars Year 28) global dust event (GDE) using data from the Mars Climate Sounder (MCS) [3]. The polar regions are fundamental to the global CO_2 cycle on Mars, controlling the $\sim$30% annual variation in total atmospheric mass, and buffering mean surface pressures. Therefore, changes in the polar regions induced by GDE could have measurable effects on the climate elsewhere on the planet.

Previous work demonstrated that GDE cause changes in atmospheric and surface temperatures [e.g., 9]. During dust storms, nighttime surface temperatures are elevated due to enhanced downwelling IR radiation from the aerosol particles. Conversely, daytime surface temperatures are reduced as a consequence of the absorbed solar radiation. During GDE, scattering by atmospheric dust increases the planetary albedo by 10's of percent [4]. We hypothesize that the enhanced planetary albedo dominates the change in overall energy balance during GDE, reducing the net absorbed heat of the system and cooling the planet. In this scenario, developed further below, polar CO_2 snowfall increases through reduced meridional sensible heat transport, along with greater availability of condensation nuclei for CO_2 cloud growth and precipitation.

Data and Methods

We used data from the Mars Climate Sounder [3] onboard NASA's Mars Reconnaissance Orbiter, consisting of infrared and solar radiance, retrieved atmospheric and surface temperatures, and aerosol opacity profiles of H_2O ice, dust, and CO_2 ice [5]. Polar snow clouds are common in polar winter, and contribute typically $\sim 10-20\%$ of seasonal deposits [6, 7]. The amount and dustiness of snowfall can significantly affect polar heat budgets, which in turn have consequences for the planetary climate [8].

Results

Patterns of cloud activity

CO_2 cloud opacity profiles retrieved from MCS radiance data show consistent patterns of snowfall in both polar regions (Fig. 1). Cloud activity generally begins after $L_S = 195°$ in the north, and $L_S = 15°$ in the south. At the onset of winter, clouds are highly concentrated near the surface (< 10 km altitude), with higher altitude clouds ($15-30$ km) becoming more prominent during mid-winter. Following the mid-winter soltical pause in the north ($L_S = 270°$), a second flurry of cloud activity occurs during $L_S = 295-345°$ at altitudes < 10 km. A similar second phase does not occur in the south.

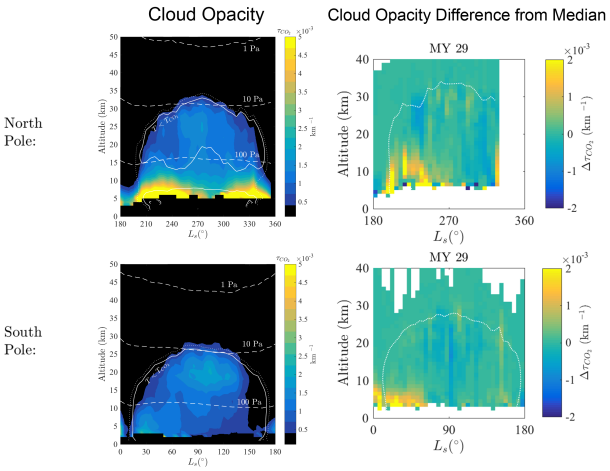

Figure 1: (left column) Median CO_2 cloud opacity profiles from MCS for MY 29 – 34 in the north (top) and south (bottom) polar winter regions $80-90°$ latitude. Colors indicate aerosol opacity, and the horizontal axis is L_S. Dashed lines are pressure contours. Solid curves indicate the CO_2 frost point, T_{CO2}, while dotted lines indicate $T_{CO2}+2$ K. (right column) Difference of MY 29 cloud opacity from the 5-year median, showing an enhancement in low-altitude clouds at both poles.

Changes in CO_2 clouds following the MY 28 GDE

Following the Mars Year (MY) 28 global dust event, we observed distinct changes in the amount of CO_2 cloud activity appearing in the MCS retrievals in the winters of MY 29 (Fig. 1). Enhanced cloud opacity occurred in both winter hemispheres during the first phase ($L_S = 195 - 265°$) of low-altitude activity. Although a data gap prevents a complete analysis, the north polar region's second phase ($L_S = 295 - 345°$) appears to show signs of enhanced activity as well. Notably, although the south polar region typically does not exhibit a second phase of low-altitude activity, the MY 29 data do show slightly elevated CO_2 cloud opacity around $L_S = 115 - 165°$.

The increase in low-altitude cloud activity during MY 29 is contrasted with a net decrease in clouds in the middle troposphere. Around the solsticial pause in both winter hemispheres, the polar cloud activity at altitudes 10 - 30 km is reduced or nearly the same as in other years. Based on the difference of MY 29 cloud opacity from the 6-MY median (MY 29 - 34), both poles show an enhancement of $\sim 50\%$ during their respective winters following the MY 28 GDE.

Changes in snowfall

Effects of the MY28 GDE can also be seen in the amount of snowfall occurring in the following winter seasons. Surface brightness temperatures at 32 μm ($T_{32\mu}$) retrieved from MCS behave as a proxy for snowfall occurrence, owing to the strong emissivity reduction of granular CO_2 ice in the transparency band from ~ 20 μm to 40 μm [6, 8, 11, 12]. We used $T_{32\mu}$ data for three different north polar sites at latitudes $\sim 80 - 85°$ to determine the mean deviation of years with and without dust storms. In MY 29 (following the GDE of MY 28), we found a net reduction in $T_{32\mu}$ of ~ 2 K at two of these sites, and no change at the third. Notably, the two sites exhibiting these changes were at similar latitudes ($\sim 80°$), but separated by 90° of longitude. The changes are consistent with increased snowfall at at these sites during MY 29, relative to MY 30-32.

Effects on the polar heat budget

We measured the outgoing long-wave infrared radiation (OLR) by integrating the top-of-the-atmosphere radiances from MCS. As shown in Figure 2, the southern summer of MY 29 showed a measurable drop in OLR compared to the following Mars year. This reduction in OLR is $\sim 10^{13}$ W, and appears not to be directly compensated by a rise in OLR during other seasons. Furthermore, the north pole does not show any significant difference in OLR during MY 29 compared to the following Mars year.

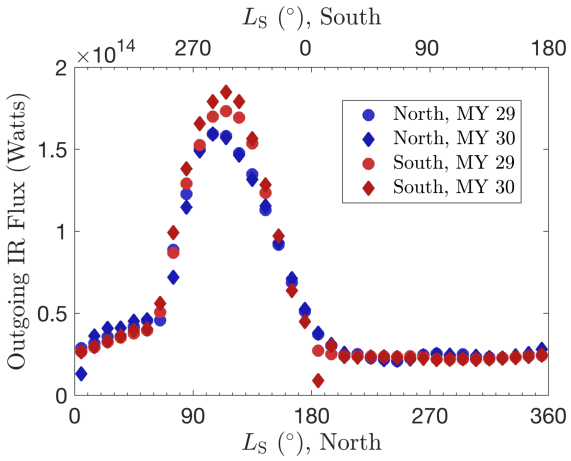

Figure 2: Outgoing long-wave radiation (OLR) from the top of the Mars atmosphere, based on average MCS brightness temperatures from 12 to 32 μm in the polar regions $> 80°$ latitude. Note the reduction of OLR during southern summer of Mars Year 29 (red circles)

The measured reduction in OLR during the south polar summer could be offset most directly by a change in the amount of CO_2 ice deposited on the surface, either through snowfall or direct frost accumulation. With a latent heat $L \approx 6 \times 10^5$ J kg^{-1} and bulk density $\overline{\rho} = (1 - \phi)\rho \approx 500$ kg m^{-3} (with $\phi \approx 0.7$ the porosity) [13], the heat deficit $\Delta Q \times \Delta t \sim (10^{13}$ W$) \times (10^7$ s) corresponds to a difference in CO_2 ice deposit thickness $\Delta z \sim \Delta t \Delta Q / (\overline{\rho} L A_{\rm cap}) \approx 10$ cm, which is roughly 10% of the mean seasonal cap thickness [13]. In order to offset the heat deficit during summer, this excess ~ 10 cm layer would accumulate during the south polar winter of MY 29. We do not observe a measurable increase in OLR during south polar winter of MY 29, and therefore the heat loss causing an increase in CO_2 deposition must be offset elsewhere. For example, the total heat deficit of $\sim 10^{13}$ W could be caused by a small increase in mean planetary albedo of $\sim 0.1\%$.

We examined the possible change in planetary albedo due to global dust storms using the optical depth data from [14], and a two-stream radiative transfer model [6, 7]. Column dust opacities exceeding $\tau_{\rm vis} = 1$ covering latitudes $\pm 45°$ persisted during the MY 28 and MY 34 GDEs for ~ 60 sols. During this period, our model results indicate the planetary albedo would have increased by $\sim 10\%$ or more (Fig. 4). On average, then, the global planetary albedo during these years would have been higher by $\sim 1\%$ relative to the Mars years without GDE. Further analysis will be carried out to improve this estimate, but these results indicate the modeled increase in planetary albedo could be sufficient to cause the observed polar heat deficit.

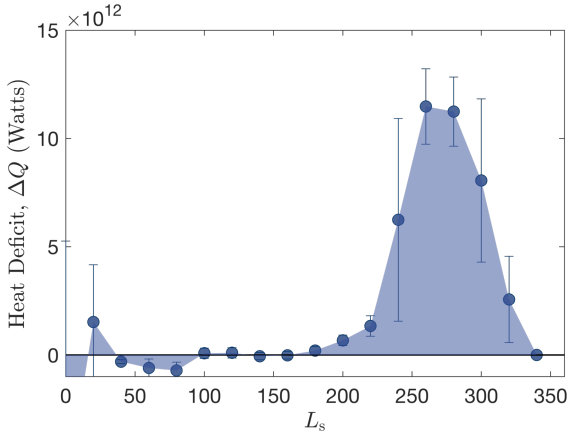

Figure 3: Heat deficit of the south polar region 80-90°S based on (negative) difference in OLR for the MY 29 summer following the MY 28 global dust event.

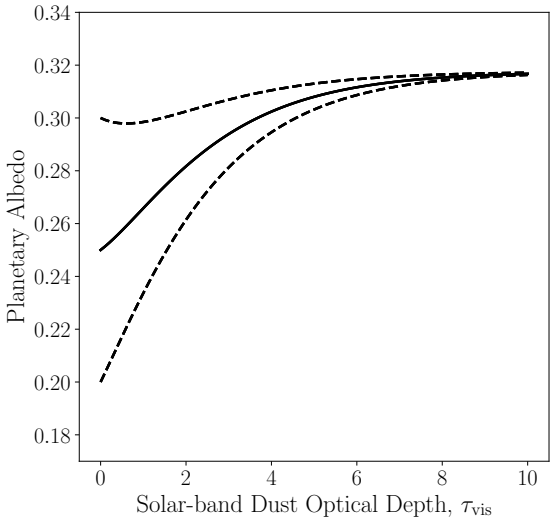

Figure 4: Modeled planetary albedo using the two-stream delta-Eddington approximation and dust solar-band single-scattering albedo ($\varpi = 0.94$) and asymmetry parameter ($g = 0.7$) from [15], as a function of atmospheric column dust optical depth. The solid line indicates the approximate global Bond albedo of Mars (under dust-free atmospheric conditions) of ~ 0.25 [16]. Dashed lines indicate the approximate range given variations in surface albedo at regional ($\sim$1,000 km) scales.

Discussion

Previous analysis of the MY 34 GDE using the LMD-MGCM and MCS data assimilation [9] found that increased dust visible optical depth reduced daytime surface radiative fluxes and lowered daytime surface temperatures, whereas nighttime temperatures were increased due to enhanced atmospheric IR optical depth. The net effect was ~ 0.9 K of warming, where the nighttime increase outweighed the daytime decrease. However, from an energy balance perspective, the net effect is one of planetary cooling. The increase in planetary albedo during a GDE reduces the solar flux at the surface by $\sim 30 - 60$ W m^{-2} (roughly 50-75% reduction in absorbed radiation) [10]. Planetary IR emission is also reduced during GDE, because a comparable reduction (within ~ 1 K) of daytime temperatures corresponds to a much larger change in thermal emission:

$$F^{\uparrow}_{\rm IR} = \sigma(T+\Delta T)^4 = \sigma T^4 + 4\sigma\Delta T T^3 + ...$$
$$\rightarrow \Delta F^{\uparrow}_{\rm IR} \sim \Delta T T^3 \ \text{ for } \Delta T \ll T$$

With $T_{\rm day} = 265$ K, $T_{\rm night} = 210$ K, and $\Delta T = 15$ K, the changes in daytime and nighttime IR fluxes are $\Delta F^{\uparrow}_{\rm day} \approx -63$ W m^{-2} and $\Delta F^{\uparrow}_{\rm night} \approx +32$ W m^{-2} respectively. The net change is therefore $\Delta F^{\uparrow}_{\rm net} \approx -31$ W m^{-2}, implying planetary cooling. With Mars' hemispheric surface area of $\sim 7\times10^{13}$ m^2, the total reduction in absorbed power could be as large as $\sim 10^{15}$ W. Thus, the observed decrease in MY 29 summer OLR (and corresponding enhancement in CO_2 deposition in the preceding winter) could be explained by the net reduction in absorbed solar radiation by the planet during the global dust storm. Sensible heat transport into the polar regions could therefore have been reduced overall during MY 29 as a result of the preceding year's dust event.

Conclusions

- Atmospheric retrievals from MCS show an increase in low-altitude polar cloud opacity of $\sim 50\%$ in both winter seasons (i.e., a full Mars Year) following MY 28 global dust storm.
- Surface brightness temperatures from indicate enhanced snowfall in the northern winter of MY 29.
- Outgoing longwave radiation was reduced by $\sim 10^{13}$ W during the south polar summer of MY 29 compared to years that did not follow a GDE.
- We show that the observed changes can be understood in terms of changes to the planetary heat budget driven by a reduction in absorbed solar radiation due to enhanced planetary albedo during periods of high atmospheric dust opacity.
- Further work, including analysis of MCS data from other GDEs and model comparisons, will elucidate the connections between the dust cycle, CO_2 cycle, and planetary heat budget.

References

[1] Heavens, N. G. et al. (2018), *Nature Astron. 2*(2), 126-132. [2] Chaffin, M. S. et al. (2021), *Nature Astron. 5*(10), 1036-1042. [3] McCleese, D. J. et al. (2007), *JGR, 112*(E5). [4] Mallama, A. (2007), *Icarus, 192*(2), 404-416. [5] Kleinböhl, A. et al. (2009), *JGR, 114*(E10). [6] Hayne, P. O. et al. (2012), *JGR, 117*(E8). [7] Hayne, P. O. et al. (2014), *Icarus, 231*, 122-130. [8] Gary-Bicas et al. (2020), *JGR, 125*(5), e2019JE006150. [9] Streeter, P. M., et al. (2020), *GRL, 47*(9), e2019GL083936. [10] Read, P. L. et al. (2016), *Quart. J. Royal Met. Soc., 142*(695), 703-720. [11] Kieffer, H. H. et al. (2000), *JGR 105*(E4), 9653-9699. [12] Hansen, G. B. (1999), *JGR, 104*(E7), 16471-16486. [13] Aharonson, O. et al. (2004), *JGR, 109*(E5). [14] Montabone, L. et al. (2015), *Icarus, 251*, 65-95. [15] Wolff, M. J., et al. (2009), *JGR, 114*(E2). [16] Christensen, P. R. et al. (2001), *JGR, 106*(E10), 23823-23871.